International Journal for Innovation Education and Research

ONLINE ISSN: 2411-2933 PRINT - ISSN: 2411-3123

Higher-Order Accurate Finite Volume Discretization of the Three-Dimensional Poisson Equation Based on An Equation Error Method

YAW KYEI

Abstract

Efficient higher-order accurate finite volume schemes are developed for the threedimensional Poisson's equation based on optimizations of an equation error expansion on local control volumes. A weighted quadrature of local compact fluxes and the flux integral form of the equation are utilized to formulate the local equation error expansions. Efficient quadrature weights for the schemes are then determined through a minimization of the error expansion for higher-order accurate discretizations of the equation. Consequently, the leading numerical viscosity coefficients are more accurately and completely determined to optimize the weight parameters for uniform higher-order convergence suitable for effective numerical modeling of physical phenomena. Effectiveness of the schemes are evaluated through the solution of the associated eigenvalue problem. Numerical results and analysis of the schemes demonstrate the effectiveness of the methodology.

Keyword: Finite volume, local control volume, equation error expansion, uniform higherorder accurate convergence,

Published Date: 6/30/2018 **Page.107-123** **Vol 6 No 06 2018**

DOI: https://doi.org/10.31686/ijier.Vol6.Iss6.1076

Higher-Order Accurate Finite Volume Discretization of the Three-Dimensional Poisson Equation Based on An Equation Error Method

YAW KYEI
Department of Decision Sciences
North Carolina Central University
DURHAM, NC 27707,

Abstract

Efficient higher-order accurate finite volume schemes are developed for the threedimensional Poisson's equation based on optimizations of an equation error expansion on local control volumes. A weighted quadrature of local compact fluxes and the flux integral form of the equation are utilized to formulate the local equation error expansions. Efficient quadrature weights for the schemes are then determined through a minimization of the error expansion for higher-order accurate discretizations of the equation. Consequently, the leading numerical viscosity coefficients are more accurately and completely determined to optimize the weight parameters for uniform higher-order convergence suitable for effective numerical modeling of physical phenomena. Effectiveness of the schemes are evaluated through the solution of the associated eigenvalue problem. Numerical results and analysis of the schemes demonstrate the effectiveness of the methodology.

Key words. Finite volume, local control volume, equation error expansion, uniform higherorder accurate convergence, local residual error, three-dimensional Poisson's equation, local compact fluxes, flux integral formulation

1. Introduction

The problems of interest in this work have been extensively investigated and we describe some of the relevant research. Higher order compact schemes for elliptic equations have been well-investigated, [5,23,25–28], since they achieve high-order accuracies without significant increases in the bandwidths of the coefficient matrices. In [19,25,27], and other application problems [6,17,31], the univariate Taylor series expansion is used to derive the finite difference approximations of individual terms of the differential equation and then coupled to obtain the schemes for multiple spatial dimensions. Subsequently, truncation errors are formulated to assess the accuracies of the schemes.

In [12,13], the multivariate Taylor expansion is used in developing higher-order finite volume schemes for elliptic equations in two spatial dimensions. First, local approximations for the unknown and the source are utilized to formulate an equation error expansion for the integral form of the equation. Generalized weighted quadratures of the local approximations are utilized for the equation error expansions based on flux integral formulations of the equation in order to capture all local compact fluxes and preserve operator

properties of the equation within the computational domain. The weight parameters are subsequently determined to minimize this wellbalanced error by eliminating the leading terms of the error. As a result, the leading coefficients of the resulting residuals which are the numerical viscosity coefficients are consequently more accurately and completely determined for the computational domain. These viscosity coefficients which describe the growth rates of local residual errors are then optimized by right choices of quadrature weights for the schemes to ensure uniformly diminishing residual errors. In [11], the approach was extended to develop a space-time finite volume differencing framework for effective higher-order accurate discretizations for parabolic equations.

In this paper, we utilize the local equation error expansion approach [11–13] to develop higher-order accurate discretizations for the three-dimensional Poisson's equation based on approximations of the flux integral formulations of the equation.

This ensures that the resulting residual errors are more accurately and completely determined for optimal quadrature weights for the discrete equations and further guarantee uniformly converging residual errors. That is, the focus is on the efficient representation of both the solution and the source term in the discrete representations of the equations. Our work in [11,12] shows that the rates of higher-order accurate convergence of the solution depends on efficient discretization of the source term in the discrete representation of the equation. While the 19-point stencil and the 27point stencil may be used for the solution [14,25,27], the associated stencils to be used for the source term should be emphasized as either the 7-point stencil or the 19-point stencil or the 27-point stencil. By using the equation error expansion which combines all local compact fluxes of the solution and their corresponding source term approximations in describing the resulting residual errors, the errors associated with all the various stencils for the source term may be optimally assessed. The weighted quadrature descriptions express the approximation of the divergence of the flow about each point within the computational domain and offers the right framework to allow for effective local flux improvements to ensure more uniform higher-order accuracies. Hence, there is effective representation of fluxes to neighboring grid points which ensures conservation of flow within the computational domain.

The equation error expansions allow for flexible configurations of local grid-point clouds [7,10,16] to be adopted as desired in order to effectively approximate fluxes in all compact directions of neighboring grid points needed to account for high frequencies in data distributions [15,30]. The structured distribution of grid points [1] ensures that accuracy estimates of the local residual error can be guaranteed. Thus, a local equation error [2] is formulated for the integral formulation of the equation on the control volume instead of just the coordinate directions as in traditional finite difference formulations [19,25]. This error is then locally constrained by the derivatives of the equation through the Cauchy-Kovalevskaya procedure [20] and then minimized by eliminating the leading terms iteratively to determine the weights to approximate the equation. These weights are further optimized to control the growth of residual errors and ensure uniformly diminishing computational errors and robust higher-order accurate convergence of the schemes.

The paper is organized as follows: In Section 2, we present the discretization framework of the method for a general elliptic equation in flux divergence form in ^{2}. In Section 3, we apply the method to develop new efficient higher-order schemes for the three-dimensional Poisson equation. We discuss quadrature-weight

optimizations of the residual errors for consistent fourth-order convergence for the resulting schemes in Section 4. In Section 5, we apply the resulting schemes to discuss the solution of the associated eigenvalue problem for the unit cube to demonstrate the efficiency of the numerical schemes. Numerical errors for the eigenvalue problem associated with different local stencil supports for the discretizations are demonstrated in Section 6. Sixth-order accurate discretizations for the three-dimensional Poisson equation is discussed in Section 7 and conclusions are presented in Section 8.

2. Finite Volume Differencing Discretization Framework

We describe the finite volume differencing discretization method for the elliptic boundary value problem

$$-\nabla \cdot (\kappa \nabla u) = q, \quad \text{in} \in \Omega \qquad (2.1)$$

$$u = g, \quad \text{on} \in \Gamma \qquad (2.2)$$

where Ω is a bounded domain in ^{2} or ^{3} with a smooth boundary Γ. We assume that $\kappa \in L^\infty(\Omega)$ is positive and the source function $q \in L^2(\Omega)$.

To develop a higher-order accurate discretization for (2.1) with a robust computational convergence, the discretization framework must effectively be able to represent all local fluxes to as many neighboring grid points as possible within the computational domain. That is, the framework must be conservative of all local compact fluxes [4] required for consistent and robust higher-order accuracies. We therefore formulate the equation (2.1) over local control volumes which can support all possible local fluxes to neighboring mesh points rather than independently in univariate coordinate directions [24] as in traditional finite difference formulations.

We first write the integral formulation of the equation (2.1) as

$$-\int_\Omega \nabla \cdot \kappa \nabla u \, dv = \int_\Omega q \, dv \qquad (2.3)$$

where $dv = dxdy$ in ^{2} or $dv = dxdydz$ in ^{3}. By the divergence theorem, the equation (2.3) is rewritten into the flux integral balance form as

$$-\int_{\partial\Omega} \kappa \nabla u \cdot \nu \, dS = \int_\Omega q \, dv \qquad (2.4)$$

where v is the unit outward normal to the boundary S of the domain Ω.

Now, consider the domain Ω partitioned into control volumes where each control volume is identified by its centroid mesh point and a distribution of neighboring mesh points. A uniform distribution of grid points is utilized for this work but the approach is applicable for a non-uniform distribution as well. A combination of uniform distribution for regular grid points and non-uniform distribution for irregular grid-points may be adopted [6]. The grid-point clouds for neighboring control volumes overlap [29] to create interlocking configurations which help to capture and track local fluxes effectively on the computational domain necessary for higher level of conservation and robust higher-order computational convergence.

We thus describe (2.4) about the centroid of each control volume $\mathbf{Q}_h$ by

$$-\int_{\partial \mathbf{Q}_h} \kappa \nabla u \cdot \nu_h \, dS_h = \int_{\mathbf{Q}_h} q \, dv \qquad (2.5)$$

where v_h is the unit outward normal vector to S_h which is the boundary of $\mathbf{Q}_h$. The equation (2.5) represents the conservation of u about the centroid grid point of the control volume such that variations in the local source term distribution within the control volume are compensated for by the radial fluxes through the boundary S_h [9]. That is, the distribution of u within the control volume $\mathbf{Q}_h$ is completely determined by the sum of all diffusive radial fluxes about the centroid and the corresponding source term distribution. Hence the resulting equation error $E(u)$, about the centroid grid point is given by

$$E(u) = -\int_{\partial \mathbf{Q}_h} \kappa \nabla u \cdot \nu_h \, dS_h - \int_{\mathbf{Q}_h} q \, dv \; = 0 \quad , \qquad (2.6)$$

where $\mathbf{Q}_h$, a typical control volume in ^{2} with a centroid $X_0(x_m,y_n)$, is described as $\mathbf{Q}_h = [x_m-h,x_m+h]\times[y_n-h,y_n+h]$ and illustrated by Figure 2.1. In illustrating the control volume $\mathbf{Q}_h$ with centroid X_0 by a finite cloud of quadrature points $X_1(x_m +$

$$h, y_n),\ X_2(x_m + h, y_n + h),\ X_3(x_m, y_n + h),\ X_4(x_m - h, y_n + h),\ X_5(x_m - h, y_n$$

^{3}),

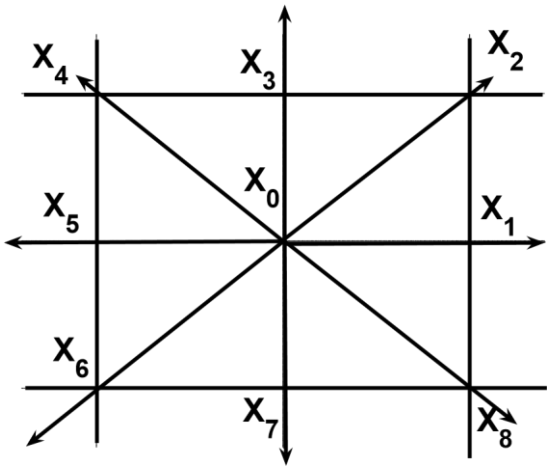

Fig. 2.1. *Local Control Volume,* $\mathbf{Q}h$ *in* ^{2}*, illustrating local compact fluxes to neighboring quadrature points within the computational domain with* $X_0(xm,yn)$ *as the centroid*

$X_6(x_m - h,y_n - h)$, $X_7(x_m,y_n - h)$, and $X_8(x_m + h,y_n = h)$, as in Figure 2.1, $\mathbf{Q}_h$ overlaps with control volumes centered on all these neighboring quadrature points.

In utilizing a finite number of quadrature representation points on the computational domain to approximate the local equation error, the discrete representation of (2.6) is therefore nonzero. In fact, we approximate the local diffusive flux about each centroid grid point (x_m,y_n) by a generalized weighted quadrature of the radial fluxes to the neighboring cloud of quadrature points by

$$\int_{\partial \mathbf{Q}_h} \kappa(u) \nabla u \cdot \nu_h \, dS_h \approx \sum_{\partial \mathbf{Q}_h} \kappa(u_0) \nabla u \cdot \nu_h \approx \kappa(u_0) \sum_{i=1}^{n_i} w_i (u_i - u_0 \qquad) \qquad (2.7)$$

where n_i is number of quadrature points, w_i is the collocation weight for the local directional flux $\nabla u \cdot v_{hi} = (u_i - u_0)$ along the radial direction v_{hi} toward location of u_i. Based on the adopted set of compact quadrature points, the quadrature approximation of (2.4) about the centroid becomes

$$-\kappa(u_0) \sum_{\partial \mathbf{Q}_h} w_i \ (u_i - u_0) = \sum_{\mathbf{Q}_h} v_i q_i \quad , \qquad (2.8)$$

where $\kappa(u_0)$ is an averaging value of $\kappa(u)$ about the centroid. The resulting residual is described as

$$E_{Qh}(u) = -\kappa(u_0)\sum_{\partial \mathbf{Q}_h} w_i\ (u_i - u_0) - \sum_{\mathbf{Q}_h} v_i q_i, /= 0 \qquad (2.9)$$

where the weights are constrained for a consistent numerical approximations such that

$$\sum_{\partial \mathbf{Q}h} w_i = 0, \quad \sum_{\mathbf{Q}h} v_i = 1. \qquad (2.10)$$

Clearly, the framework as described in (2.8) allows for regular and non-regular distribution of quadrature points locally about each centroid adaptively.

For a more accurate modeling of the local equation error (2.9) using a generalized weighted quadrature description in [2] for instance, we adopt a natural local multivariate Taylor expansion for u about each centroid (x_0,y_0) by

$$\phi(x_0+x, y_0+y) = \sum_{m=0}^{\infty}\sum_{i+j=m}\frac{C(m,i)}{m!}\frac{\partial^m \phi}{\partial x^i \partial y^j}(x_0,y_0)x^i y^j \qquad (2.11)$$

where φ is sufficiently smooth and locally defined everywhere such that

$$\varphi(x_0,y_0) = u(x_0,y_0)$$

$$\frac{\partial^m \varphi}{\partial xi \partial yj}(x0,y0) = \frac{\partial^m u}{\partial xi \partial yj}(x0,y0).$$

Consequently, we define the local source term expansion by

$$f(x_0+x, y_0+y) = -\Delta_\kappa\left(\sum_{m=0}^{\infty}\sum_{i+j=m}\frac{C(m,i)}{m!}\frac{\partial^m \phi}{\partial x^i \partial y^j}(x_0,y_0)x^i y^j\right) \qquad (2.12)$$

where Δ_κ is the local differential operator description of (2.1) with unique characteristics of the equation [21] such that

$$q(x_0,y_0) = f(x_0,y_0) = \triangle_\kappa \phi|_{(x_0,y_0)} := (\nabla\cdot(\kappa\nabla\phi))|_{(x_0,y_0)} = \kappa\Delta\phi|_{(x_0,y_0)}. \qquad (2.13)$$

In this way, *any* grid functions of φ and the source term f about each centroid may be determined and utilized to describe the approximations the integral fluxes in (2.4) in the form of (2.8). Thus, the grid point spacings may not necessarily need to be uniform and can be adaptively determined locally. As a result, *any* desired quadrature points about the centroid may be utilized or included in the approximation of the flux integrals to discretize (2.4) locally. The radial fluxes towards the neighboring quadrature points describe their relative dependencies locally on the total flux within the computational domain and therefore weighted accordingly.

To enable effective higher-order accuracies, the Cauchy-Kovalevskayaprocedure [20] is applied to replace higher order derivatives of the local solution expansion φ in (2.11) and (2.12) by lower-order derivatives of the local source term f so that higher-order rates of change in u can be efficiently explained by local source term variations. Thus, we replace coefficients such φ_{xxxx},φ_{xxxy}, φ_{xyyy}, etc in (2.11) and (2.13) by φ_{xxyy}, etc in order to more accurately represent local directional fluxes according to the physics behind (2.1) in the local expansions. Thus, the source term derivatives f_x, f_y, f_{yy}, f_{xx}, etc are introduced into (2.11) through higher-order derivatives of the equation (2.13) given as

$$
\begin{aligned}
-\kappa(\phi_{xx}+\phi_{yy}) &= f,\\
-\kappa(\phi_{xxx}+\phi_{xyy}) &= f_x,\\
-\kappa(\phi_{xxy}+\phi_{yyy}) &= f_y,\\
-\kappa(\phi_{xxxy}+\phi_{xyyy}) &= f_{xy},\\
-\kappa(\phi_{xxxx}+\phi_{xxyy}) &= f_{xx},\\
-\kappa(\phi_{xxyy}+\phi_{yyyy}) &= f_{yy}, \text{ etc}
\end{aligned}
$$

5 .

As indicated by (2.7), the local diffusive flux about each centroid mesh point (x_0,y_0) within the computational domain is described by a generalized weighted quadrature of all local compact fluxes by

$$\int_{\partial \mathbf{Q}_h} \kappa \nabla\phi \cdot \nu_h \, dS_h \approx \kappa_{\mathbf{Q}_h} \sum_{\partial \mathbf{Q}_h} \nabla\phi \cdot \nu_h \approx \kappa_{\mathbf{Q}_h} \sum_{i=1}^{n_i} w_i(\phi_i - \phi_0 \qquad) \qquad (2.14)$$

where n_i is the desired number of quadrature points, and w_i is the quadrature weight for the local directional flux ($\varphi_i - \varphi_0$). The number of quadrature points forming the desired local distribution is part of the available degrees of freedom, which may be increased to improve local accuracy by incorporating sub-grid-scale points and nonlocal fluxes [3].

Thus, the local equation error expansion E_{Qh} about each centroid grid point is described as the differencing of the weighted quadrature approximations of the flux integrals by

$$\text{E}Qh = \quad -\kappa_{\mathbf{Q}_h} \sum_{\partial \mathbf{Q}_h} w_i(\phi_i - \phi_0) - \quad \sum v_i f_i, \qquad (2.15)$$

$$\mathbf{Q}_h$$

where the weights are constrained by

$$\sum_{i=1}^{8} w_i = 0, \quad \sum_{i=0}^{8} v_i = 1 \qquad (2.16)$$

such that the differential and integral operator properties of the equations are preserved about each centroid. This error expansion measures the sum of the discrepancies of the separate possible approximations flux integrals using subsets of the quadrature points as in traditional finite difference approximations of (2.1). Thus, the formulation (2.4) offers a more complete accounting of local fluxes than traditional finite difference approximations which is a parameterized version of this framework.

To obtain the specifics the discretization for (2.1), the discrete minimax approach is utilized to determine the quadrature weights to annihilate the leading terms of the error expansion. That is, the weights w_i and v_i are determined to annihilate the leading terms of the multivariate error expansion of (2.5) and to further regulate the growth of the residual error through efficient collocations of the local source terms f_i and the solutions φ_i. The eventual order p of the approximation depends on the degrees of freedom available to discretize the equation (2.4) locally.

One advantage here is that for various innovative ways [22,30] to incorporate local micro scale properties into the numerical model, our comprehensive approach is naturally efficient in determining the right sampling and collocations of the source required for effective and robust higher-order accuracy.

3. Finite Volume Discretization for Poisson's Equation in 3D

We formulate the equation error expansion (2.9) about each grid point using local compact cloud of 27 grid points within the three-dimensional computational domain. The corresponding control volume Q_h, for a uniformly partitioned computational domain is illustrated in Figure 3.1 where the centroid grid-point function φ_0, is surrounded by 26 mesh points distributed at three radial distances of $h,\ \sqrt{2}h$ and$\sqrt{3}h$ from the centroid.

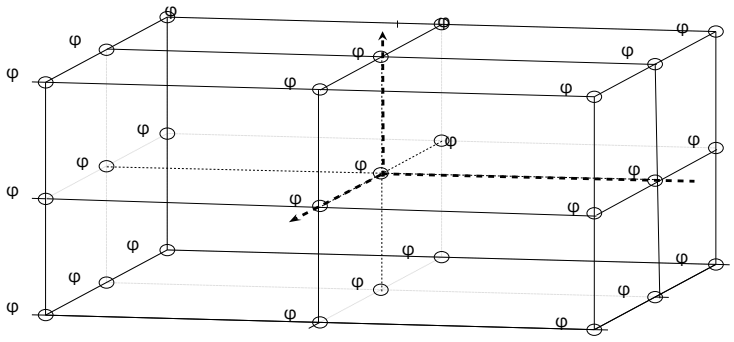

Fig. 3.1. *A compact cloud of neighboring grid-point distribution about each Centroid*

As discussed above, we use the multivariate Taylor expansion $\varphi(x_0 + \alpha, y_0 + \tau, z_0 + \nu)$ defined in the form of (2.11) for the local expansion of the solution about each centroid. In a likewise manner, the local source term is formulated on the local stencil by a corresponding multivariate expansion as described by 3*D* versions of (2.11), (2.12) and (2.13). Thus, the compact stencil grid point approximations are well defined for φ_i and their corresponding source terms f_i everywhere about the centroid.

For a regular uniform discretization of size *h*, we define and evaluate the local compact cloud of grid-point approximations of φ_i about the centroid by

$$\begin{array}{llll}
\phi_0 = \phi(0,0,0), & \phi_1 = \phi(h,0,0), & \phi_2 = \phi(0,h,0), & \phi_3 = \phi(-h,0,0) \\
\phi_4 = \phi(0,-h,0), & \phi_5 = \phi(0,0,h), & \phi_6 = \phi(0,0,-h), & \phi_7 = \phi(h,h,0), \\
\phi_8 = \phi(-h,h,0), & \phi_9 = \phi(-h,-h,0), & \phi_{10} = \phi(h,-h,0), & \phi_{11} = \phi(h,0,h) \\
\phi_{12} = \phi(0,h,h) & \phi_{13} = \phi(-h,0,h) & \phi_{14} = \phi(0,-h,h), & \phi_{15} = \phi(h,0,-h) \\
\phi_{16} = \phi(0,h,-h) & \phi_{17} = \phi(-h,0,-h) & \phi_{18} = \phi(0,-h,-h), & \phi_{19} = \phi(h,h,h) \\
\phi_{20} = \phi(-h,h,h) & \phi_{21} = \phi(-h,-h,h) & \phi_{22} = \phi(h,-h,h) & \phi_{23} = \phi(h,h,-h) \\
\phi_{24} = \phi(-h,h,-h) & \phi_{25} = \phi(-h,-h,-h) & \phi_{26} = \phi(h,-h,-h) &
\end{array}$$

as well as the source term evaluations $\{f_i\}i_{=0,2,\ldots,26}$. The equation error expansion about the centroid is then constituted as

$$E(\phi_0) = -\kappa_{\phi_0}\left\{\sum_{i=1}^{6} w_1(\phi_i - \phi_0) + \sum_{i=7}^{18} w_7(\phi_i - \phi_0) + \sum_{i=19}^{26} w_{19}(\phi_i - \phi_0)\right\} \quad (3.1)$$
$$-\left\{\beta_1 \sum_{i=1}^{6} f_i + \beta_7 \sum_{i=7}^{18} f_i + \beta_{19} \sum_{i=19}^{26} f_i + (1 - 6\beta_1 - 12\beta_7 - 8\beta_{19}) f_0\right\}$$

where equal quadrature weights are adopted for grid points at equal radial distances from the centroid. By substituting $\{\varphi_i\}i_{=0,2,\ldots,26}$ and $\{f_i\}i_{=0,2,\ldots,26}$ into threedimensional version of (2.15), the terms of the error expansion of (3.2) are assembled in the form

$$E(\phi_0) \approx \kappa U_2 \left\{ \frac{\partial^2 \phi}{\partial x^2} + \frac{\partial^2 \phi}{\partial y^2} + \frac{\partial^2 \phi}{\partial z^2} \right\} + F_2 \left\{ \frac{\partial^2 f}{\partial x^2} + \frac{\partial^2 f}{\partial y^2} + \frac{\partial^2 f}{\partial z^2} \right\} h^2$$
$$+\kappa U_4 \left\{ \frac{\partial^4 \phi}{\partial x^2 \partial y^2} + \frac{\partial^4 \phi}{\partial x^2 \partial z^2} + \frac{\partial^4 \phi}{\partial y^2 \partial z^2} \right\} h^2 + O(h^4) \quad (3.2)$$

7

where

$U_2 = 1 - w_1 - 4w_7 - 4w_{19}$

$$F2 = \beta 1 + 4\beta 7 + 4\beta 19 - \frac{1}{12} w1 - \frac{1}{3} w7 - \frac{1}{3} w19$$

$$U4 = \frac{1}{6} w1 - \frac{1}{3} w7 - \frac{4}{3} w19.$$

By annihilating the leading coefficients U_2, F_2 and U_4 of the error (3.2), the quadrature weights for the stiffness matrix **H** of the discretization are transformed as functions of w_{19} by

$$w0 = 2 + {}_h 2w19 \; {}_h \frac{4}{} \frac{8}{}$$

$$\frac{1}{} \frac{4}{} w1 = -3h2 - {}_h 2w19$$

$$1 \quad 2 \; w_7 = -2 + {}_h 2w_{19} \quad (3.3) \quad \frac{}{} \quad \frac{}{}$$

$6h$

where w_0 is the weight of centroid value φ_0. Consequently, the quadrature weights for the mass matrix **Q** are transformed as functions of β_7 and β_{19} by

$$\beta_0 = \frac{1}{2} + 12\beta_7 + 16\beta_{19}$$

$$\beta_1 = \frac{1}{12} - 4\beta_7 - 4\beta_{19} \quad (3.4)$$

and the leading terms of the local residual error $R_{\varphi 0}$, are transformed as

$$R_{\phi_0} \approx \left\{ \frac{1}{240} \left(\frac{\partial^4 f}{\partial x^4} + \frac{\partial^4 f}{\partial y^4} + \frac{\partial^4 f}{\partial z^4} \right) + \kappa \left(\frac{1}{30} - w_{19} \right) \frac{\partial^6 u}{\partial x^2 \partial y^2 \partial z^2} \right\} h^4$$
$$+ \left\{ \left(\beta_7 + 2\beta_{19} - \frac{1}{90} \right) \left(\frac{\partial^4 f}{\partial x^2 \partial y^2} + \frac{\partial^4 f}{\partial x^2 \partial y^2} + \frac{\partial^4 f}{\partial x^2 \partial z^2} \right) \right\} h^4$$
$$+ \left\{ \frac{11}{60480} \left(\frac{\partial^6 f}{\partial x^6} + \frac{\partial^6 f}{\partial y^6} + \frac{\partial^6 f}{\partial z^6} \right) + L_6 \left(\frac{\partial^6 f}{\partial x^2 \partial z^4} + \cdots + \frac{\partial^6 f}{\partial y^2 \partial z^4} \right) \right\} h^6$$
$$+\kappa L_7 \frac{\partial^6 f}{\partial x^2 \partial y^2 \partial z^2} h^6 - \frac{\kappa}{3024} \left\{ \frac{\partial^8 u}{\partial x^4 \partial y^4} + \cdots + \frac{\partial^8 u}{\partial y^4 \partial z^4} \right\} h^6 + C_6 h^8 \quad (3.5)$$

where

$$L6 = \beta 7 + \beta 19 - \frac{1}{12} \frac{1}{6} \frac{5}{12096}$$

$$L7 = \frac{5}{6048} - \frac{1}{12} w19 + \beta 19.$$

As indicated in [13], diagonal dominance of **H** requires W_{19} to be chosen to satisfy

$$|4 + 8w_{19}| \geq 6| - \frac{1}{3} - 4w_{19}| + 12|2w_{19} - \frac{1}{6}| + 8|w_{19}| \quad (3.6)$$

for which the solution is found to be

$$0 \leq w_{19} \leq \frac{1}{12}. \quad (3.7)$$

Clearly, there are several possible ways to choose $\{w_7, w_{19}, \beta_7, \beta_{19}\}$ for a fourthorder accuracy. In the next section, we discuss the optimization of such choices for higher-order convergence robustness of the discretization.

4. Residual Error Optimization for Robust Higher-order Accurate Convergence

For a uniform distribution of quadrature grid points as illustrated in Figure 3.1, higher-order accurate computational performances of the resulting schemes depend on the structure and convergence properties of the local residual error. That is, analysis of computational performances are focused on the asymptotic nature of the associated local residual errors for the equation error expansions which are of the form

$$R_{\phi_0} \approx \sum_{i,j,k}^{i+j+k=3} E_i \frac{\partial^6 \phi}{\partial x^{2i} \partial y^{2j} \partial z^{2k}} h^4 + \sum_{i,j,k}^{i+j+k=4} F_i \frac{\partial^8 \phi}{\partial x^{2i} \partial y^{2j} \partial z^{2k}} h^6 + O(h^8) \quad (4.1)$$

where the leading coefficients E_i and F_i are functions of the quadrature weights as described in (3.5). Thus, with the introduction of higher-order derivatives of f, the residual of the equation error expansion is reconstituted to describe errors in approximating the local manifold of the solution along the directions of local quadrature points.

Now, the point-wise equation error residuals for the Poisson equation and its higher-order derivatives are of the form

$$L(\varphi_0) = \varphi_{xx} + \varphi_{yy} + \varphi_{zz} + f = 0$$

$$\frac{\partial p}{\partial x^i \partial y^j \partial z^k} L(\varphi 0) = \frac{\partial p}{\partial x^i \partial y^j \partial z^k} \{\varphi xx + \varphi yy + \varphi zz + f\} = 0 \quad (4.2)$$

where $p = 1,2,3,\cdots$ and $i + j + k = p$. Notice that the coefficients of higher-order derivatives of φ and f have same signs. For the resulting discretization to produce robust higher-order computational convergence rates, the computational errors must diminish monotonically. After incorporating higher-order derivatives of the equation, the residual error terms assume the form of (4.2). Therefore, robust higher-order computational convergence requires that the coefficients of the higher-order derivatives of both φ and f within the leading terms of the residual error (4.1) maintain similar signs as described in (4.2). Thus, the weights β_7, β_{19} and w_{19} as in the leading term of the residual error expansion (3.5) should be chosen such that

$$\beta_7 + 2\beta_{19} - \frac{1}{90} \geq 0, \text{ and } \frac{1}{30} - w_{19} \geq 0 \quad (4.3)$$

to render the leading term of the residual error decreasing monotonically as resolution is refined.

5. Laplacian Eigenvalue Approximations

To computationally evaluate the higher-order accurate convergence of the resulting schemes, consider the associated eigenvalue problem for the three-dimensional Laplacian

$$-\Delta u = \lambda u, \quad \text{in} \in \Omega \tag{5.1}$$

$$u = 0, \quad \text{on} \in \Gamma \tag{5.2}$$

where Ω is the unit cube [0 1] × [0 1] × [0 1]. As discussed above, the equation error for (5.1) about the centroid of each control volume $\mathbf{Q}_h \in \Omega$ as described in (2.6) is

$$R(u) = -\int_{\partial \mathbf{Q}_h} \nabla u \cdot \nu_h \, dS_h - \lambda \int_{\mathbf{Q}_h} u \, dv \; = 0 \tag{5.3}$$

9

The finite dimensional representation of (5.3) by utilizing the local uniform cloud of quadrature points on the control volume shown in Figure 3.1 may be described as

$$\mathbf{H}\Phi - \Lambda \mathbf{Q}\Phi = \mathbf{E}R_{\varphi 0} \tag{5.4}$$

where Φ is a column vector of the discrete representation of the eigenfunctions on Ω which are locally supported by the quadrature points on the control volumes and Λ as the matrix of associated eigenvalue estimates. The mass and stiffness for the discretizations are **Q** and **H** respectively, and **E** is a column vector of ones. As described by the discrete approximation (5.4), the robustness of the resulting numerical schemes for higher-order accuracy depends on the convergence properties of the local residual error $R_{\varphi 0}$ in convergence analyses. The eigenvalue estimates, Λ and the associated eigenfunctions Φ are a function of the geometry of the domain and the boundary conditions [8]. Therefore, the accuracy of the estimates Φ and Λ are a direct reflection of the level of effectiveness of the discretization method in sufficiently approximating the equation on the geometry of the domain [18]. Thus, the effectiveness of the discretization for higher-order accuracies may be evaluated through the convergence properties of the local residual error R_{Q0} as described in (3.5).

The parameters w_{19}, β_7, and β_{19} are free for a fourth-order accuracy and so various strategies may be adopted to further optimize the discretization for convergence robustness. Since the local residual error R_{Q0} serves as the local source term for the discrete error equation associated with the discretization, our strategy for robustness is to effectively ensure that R_{Q0} is more uniformly diminishing by choosing the parameters to avoid fluctuations about zero. The computational profiles of various choices of w_{19}, β_7, and β_{19} for higher-order accurate convergence are discussed for the solution of (5.4) by the *eigs* function in *Matlab.*

6. Numerical Errors for Different Local Stencil Supports

In this Section, we discuss numerical results for the eigenvalue estimates associated with the different choices of the local computational supports for the stiffness and mass matrix pair in the discrete equation (5.4). That is, we examine the computations errors in estimating the eigenvalues of the unit cube associated with the possible choices of the parameters w_{19}, β_7, and β_{19} in (5.4).

6.1. Nineteen-by-Seven-Point Local Stencil Support for H × Q. First, the traditional finite difference scheme [19,25,27], is recovered with $w_{19} = 0$, $\beta_7 = 0$, and $\beta_{19} = 0$ in (3.5) and uses a 19×7 point local support for **H**×**Q** and the associated local residual error is given as

$$\begin{aligned} R_{\phi_0} \approx & \left\{ \frac{1}{240}\left(\frac{\partial^4 f}{\partial x^4}+\frac{\partial^4 f}{\partial y^4}+\frac{\partial^4 f}{\partial z^4}\right)+\frac{\kappa}{30}\frac{\partial^6 u}{\partial x^2\partial y^2\partial z^2}\right\} h^4 \\ & -\frac{1}{90}\left(\frac{\partial^4 f}{\partial x^2\partial y^2}+\frac{\partial^4 f}{\partial x^2\partial y^2}+\frac{\partial^4 f}{\partial x^2\partial z^2}\right) h^4 \\ & +\left\{ \frac{11}{60480}\left(\frac{\partial^6 f}{\partial x^6}+\frac{\partial^6 f}{\partial y^6}+\frac{\partial^6 f}{\partial z^6}\right)-\frac{5}{12096}\left(\frac{\partial^6 f}{\partial x^2\partial z^4}+\cdots+\frac{\partial^6 f}{\partial y^2\partial z^4}\right)\right\} h^6 \\ & +\frac{5\kappa}{6048}\frac{\partial^6 f}{\partial x^2\partial y^2\partial z^2}h^6-\frac{\kappa}{3024}\left\{\frac{\partial^8 u}{\partial x^4\partial y^4}+\cdots+\frac{\partial^8 u}{\partial y^4\partial z^4}\right\} h^6+C_6h^8. \qquad (6.1) \end{aligned}$$

Clearly, condition (4.3) fails with both $O(h^4)$ and $O(h^6)$ terms having both positive and negative signs. The computational error profile illustrated by Figure 6.1 shows considerable inconsistent accuracy performances for the eigenvalues due to nonsystematic cancelations of error terms for all eigenfunctions. Furthermore, since the local support for **Q** is a 7-point stencil while that of **H** is a 19−point stencil, some eigenfunctions are poorly and inconsistently represented. Hence the differing shapes of the eigenfunctions along different directions affect the accuracies of their approximations differently.

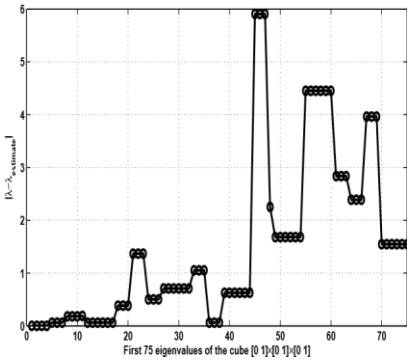

Fig. 6.1.
Computational errorsfirst the 75 eigenvalues of the unit cube$|\lambda - \lambda_{estimate}|$ for
with 19 × 7 point local support, illustrated in Figure 6.1.

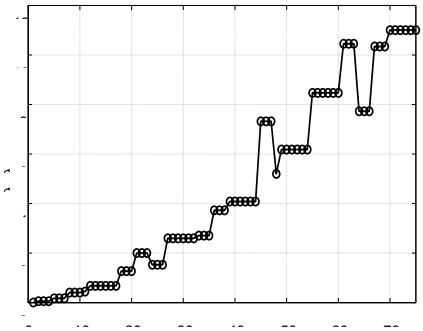

Fig. 6.2.
Computational errors $|\lambda - \lambda_{estimate}|$ for first the 75 eigenvalues of unit the cube with 19 19 point local support,

6.2. Nineteen-by-Nineteen-Point Local Stencil Support for H × Q. On the other hand, in utilizing a 19−point local support for both the mass matrix **Q** and the stiffness matrix **H** by choosing $w_{19} = 0$, $\beta_7 \neq 0$, and $\beta_{19} = 0$ in (3.5), seems geometrically logical. A direct obvious choice of $\beta_7 = \frac{1}{90}$ from (5.4) shows a more uniform convergence profile as shown in Figure 6.2 than with $\beta_7 = 0$

First 75 eigenvalues of the cube [0 1]×[0 1]×[0 1]

$w_{19} = \ _7 = \ _{19} = 0$ for $= \frac{1}{10}$ × $w_{19} = \beta_{19} = 0,\ \beta_7 = \frac{1}{90}$ $h = \frac{1}{10}$

β β $h$for

The computational errors for the eigenvalues as displayed in Figure 6.1 are clearly lower than those in Figure 6.2 for the 7−point and 19−point stencil mass matrices respectively. However, in Figure 6.2, the errors grow more uniform with the level of complexity of eigenfunctions demonstrating a more robust higher-order convergence and consistent accuracies. That is, the 19-point stencil mass matrix **Q** with

$\beta_7 = \frac{1}{90}$has a leading error expansion term with same signs for the higher-order derivatives as described in (4.2) ensuring a monotonic convergence than for the 7−point stencil mass matrix with $\beta_7 = 0$.

Furthermore, the mass matrix **Q** with $\beta_7 = \frac{3}{200}$ provides an improved uniform fourth-order accuracies than with$\beta_7 = \frac{1}{90}$ as demonstrated between Figures 6.2 and 6.3. With $\beta_7 = \frac{1}{90}$, the mixed partial derivatives of the source term *f* is eliminated from the $O(h^4)$ term and the size of the leading error term gets polluted by $O(h^6)$ term for some eigenfunctions.

A convergence analysis through resolution refinement for the 19−point stencil mass matrix **Q** with$\beta_7 = \frac{3}{200}$ is shown from Figure 6.3 with h = 1/10 to Figure 6.4 with h = 1/20 which fails to show much local improvements in the error profile. Thus, the 19−point stencil for both the mass and stiffness matrices in 3*D* is not sufficient and effective enough in generating local accuracy improvements as resolution is refined.

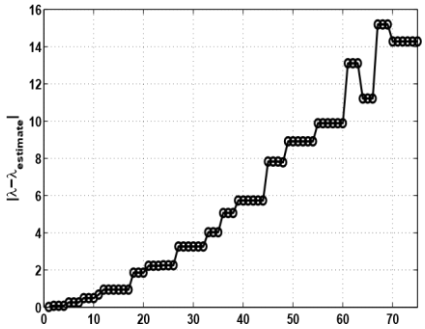

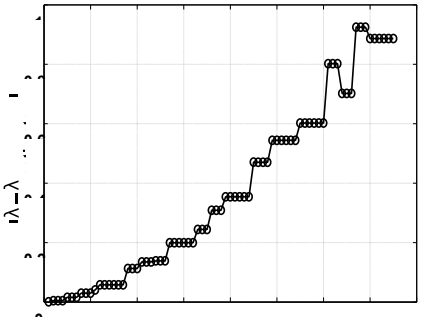

First 75 eigenvalues of the cube [0 1]×[0 1]×[0 1]First 75 eigenvalues of the cube [0 1]×[0 1]×[0 1]

Fig. 6.3. Fig. 6.4.

Computational errors$|\lambda - \lambda_{estimate}|$ for unit the cube first the 75 eigenvalues of unit the cube with 19 × 19 point local support, $w_{19} = 0$, with $\beta_7 = \frac{1.35}{90} = \frac{3}{200}$, $\beta_{19} = 0$ with $h = \frac{1}{10}$

Computational errors $|\lambda - \lambda_{estimate}|$ for first the 75 eigenvalues of 19 × 19 point local support, $w_{19} = 0$, $\beta_7 = \frac{1.35}{90} = \frac{3}{200}$, $\beta_{19} = 0$ with $h = \frac{1}{20}$

6.3. Twenty-Seven Point Stencil. Next, we examine the case for a 27−point stencil local support for the discretization. Since the parameters w_{19}, β_7, and β_{19} are free for a fourth-order accuracy as indicated by the residual error (3.5), our strategy for robustness and consistent higher-order accurate convergence is to ensure that the residual error is uniformly diminishing by reducing the size and fluctuations of the residual error as much as possible as resolution is refined. Therefore, we exercise the choices for w_{19}, β_7, and β_{19} to control leading coefficients in both the $O(h^4)$ and $O(h^6)$ terms to minimize associated local error pollution. First, we utilize w_{19} to eliminate $\partial x2^{\partial} \partial y^{6f}{}_2 \partial z_2$ in the ^{6}) term and then utilize β_{19} to eliminate $\partial x2^{\partial} \partial y^{6u}{}_2 \partial z2$ term in $O(h^4)$ $O(h$

term such that

$$w_0 = -6w_1 - 12w_7 - 8w_{19} = -\frac{64}{15h2}$$

$$w_1 = -(1 + 4w_7 + 4w_{19}) = \frac{7}{15h_2}$$

$$w_7 = -(\frac{1}{6} + 2w_{19}) = \frac{1}{10h_2}$$

$$w19 = -12\beta 19 - \frac{5}{504} = \frac{1}{30h^2} \qquad (6.2)$$

$\beta_0 = 1 - 6\beta_1 - 12\beta_7 - 8\beta_{19} = \frac{502}{945} + 12\beta_7$ which transforms the error as

$$\beta_1 = \frac{1}{12} - 4\beta_7 - 4\beta_{19} = \frac{571}{7560} - 4\beta_7$$

$$\beta_{..} = \frac{59}{30240} \qquad (6.3)$$

$$\begin{aligned} R_{\phi_0} \approx & \left\{ \frac{1}{240}\left(\frac{\partial^4 f}{\partial x^4} + \frac{\partial^4 f}{\partial y^4} + \frac{\partial^4 f}{\partial z^4}\right) + (\beta_7 - \frac{109}{15120})\left(\frac{\partial^4 f}{\partial x^2 \partial y^2} + \cdots + \frac{\partial^4 f}{\partial x^2 \partial z^2}\right)\right\} h^4 \\ & + \left\{ \frac{11}{60480}\left(\frac{\partial^6 f}{\partial x^6} + \frac{\partial^6 f}{\partial y^6} + \frac{\partial^6 f}{\partial z^6}\right) - \frac{\kappa}{3024}\left(\frac{\partial^8 u}{\partial x^4 \partial y^4} + \cdots + \frac{\partial^8 u}{\partial y^4 \partial z^4}\right)\right\} h^6 \\ & + \left(\frac{\beta_7}{12} - \frac{1}{11340}\right)\left(\frac{\partial^6 f}{\partial x^2 \partial z^4} + \cdots + \frac{\partial^6 f}{\partial y^2 \partial z^4}\right) h^6 + C_0^6(x_0, y_0, z_0) h^8. \end{aligned} \qquad (6.4)$$

For a higher-order accurate method, the objective here is to achieve a robust discretization scheme by ensuring stability and steady higher-order accurate convergence. For stability, β_7 should be selected to ensure diagonal dominance of the mass matrix **Q** such that

$$\left| 6\left|\frac{1}{7560} - 4\beta_{19}\right| + 12\beta_7 \right| + 8\left|\frac{502}{954} + 12\beta_7\right| \geq \left|\frac{571}{945} - 8\beta_{19}\right| + \left|\frac{59}{30240}\right|, \qquad (6.5)$$

the solution is determined as

$$0 \leq \beta_7 \leq \frac{1831}{45360}. \qquad (6.6)$$

For a steady and a robust higher-order accurate convergence, the choice of β_7 should be made to render the error (6.4) uniformly diminishing with same signs for the source term derivatives in the $O(h^4)$ term such that

$$\beta_7 \geq \frac{109}{15120} = \frac{327}{45360} \qquad (6.7)$$

which leads to a 27−point compact discretization for the equations.

In terms of local support, the 27−point compact stencil for both the mass and stiffness matrices provides for a complete representation of the eigenfunctions as demonstrated in a comparison of error convergence profiles in Figures 6.5 and 6.6.

As evident from Figure 6.5, resolution refinement fails to improve on local accuracies for larger eigenvalues with the 19 × 19 discretization. On the other hand, the 27 × 27 discretization shows much improvement in local accuracy as illustrated in in Figure 6.6.

Clearly, the 27−point compact local support for both the stiffness and mass matrices provide for a uniform higher-order accurate convergence rates for the eigenvalue calculations as well as consistent local improvements in accuracies as resolution is refined which is suitable for effective numerical modeling of physical phenomena.

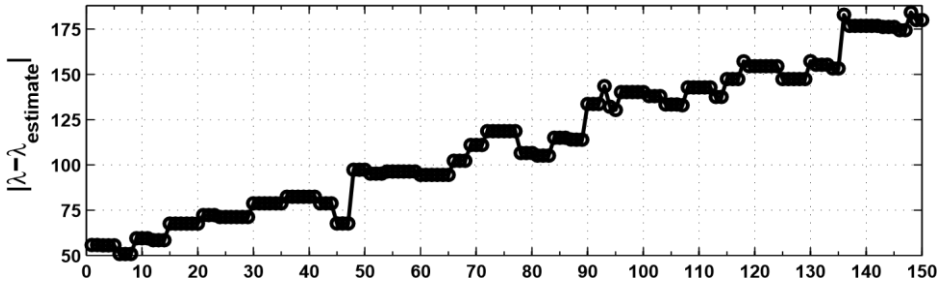

150th to 300th eigenvalues of the cube [0 1]×[0 1]×[0 1]

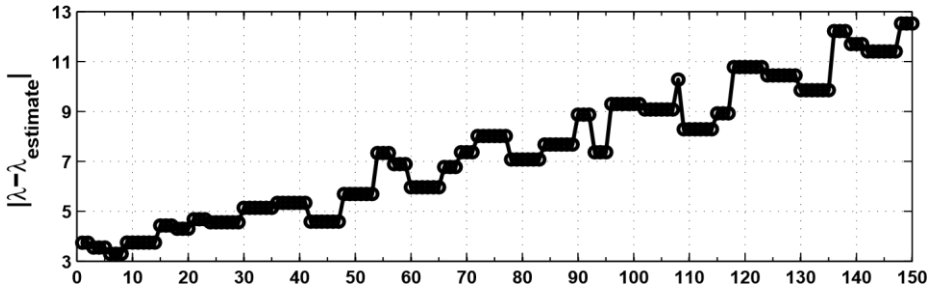

150th to 300th eigenvalues of the cube [0 1]×[0 1]×[0 1]

Fig. 6.5.

Computational errors $|\lambda - \lambda_{estimate}|$ for the 150*th* to 300*th* eigenvalues of unit the cube with 19 × 19 point local support, $w_{19} = \beta_{19} = 0$, $\beta_7 = \frac{1.35}{90} = \frac{3}{200}$, with $h = \frac{1}{10}$and $h = \frac{1}{20}$ for the top and bottom graphs respectively.

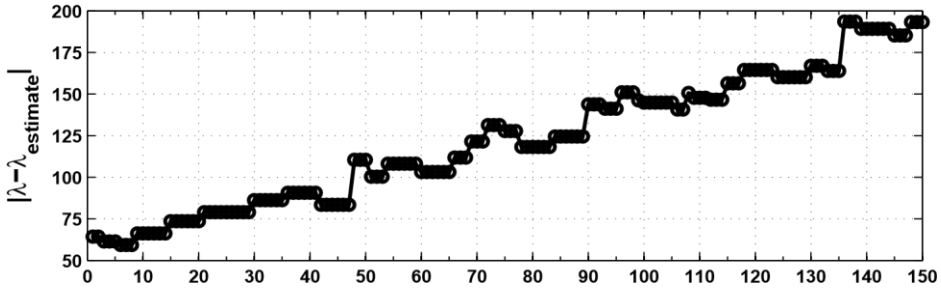

150th to 300th eigenvalues of the cube [0 1]×[0 1]×[0 1]

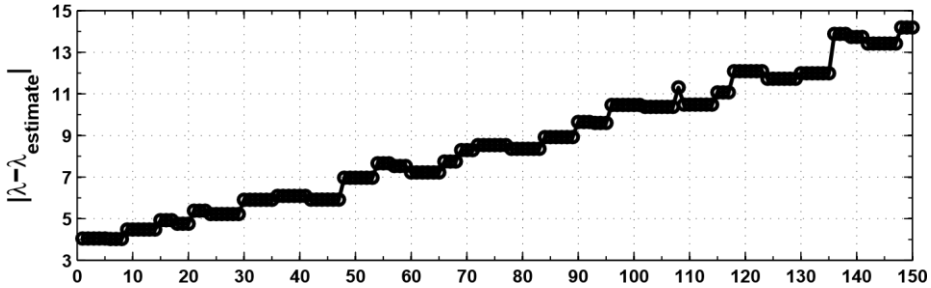

150th to 300th eigenvalues of the cube [0 1]×[0 1]×[0 1]

Fig. 6.6.

Computational errors $|\lambda - \lambda_{estimate}|$ for the 150*th* to 300*th* eigenvalues of unit the cube with 27 × 27 point local support, $w_{19} = \frac{1}{30}$, $\beta_7 = 2.3 * \frac{327}{45360} = \frac{2507}{151200}$, $\beta_{19} = \frac{59}{45360}$ with $h = \frac{1}{10}$ and $h = \frac{1}{20}$ for the top and bottom graphs respectively.

7. Sixth-Order Accuracy

Since the $O(h^4)$ term in the local residual error only involves derivatives of the source term, the right sampling of the numerical source term at sub-grid scale points on the computational stencil may be utilized to achieve sixthorder accuracy. If the fourth-order derivatives of the source term are readily available then the sixth-order accuracy may be achieved by determining β_7 to annihilate the $O(h^4)$ term in the residual error by

$$\beta_7 = \frac{109}{15120} - \frac{1}{240}\left(\frac{f_{xxxx} + f_{yyyy} + f_{zzzz}}{f_{xxyy} + f_{xxzz} + f_{yyzz}}\right). \qquad (7.1)$$

On the other hand, since

$$\mathbf{F}^{Q_h} = 18f_0 - 4f_{\frac{1}{2}} + f_{1-6} \approx \frac{f_{xxxx} + f_{yyyy} + f_{zzzz}}{240}h^4$$

$$fxxxxxx + fyyyyyy + fzzzzzz^{\,6} + \frac{}{+h} \qquad O(h^8) \qquad (7.2)$$

$$5760$$

where

$$f_{1-6} := \underset{h}{f_1} + \underset{h}{f_2} + \underset{h}{f_3} + \underset{h}{f_4} + \underset{h}{f_5} + \underset{h}{f_6}, \quad f_{7-18} := \underset{h}{f_7} \cdots \underset{h}{f_{18}} \text{ ,and}$$

$$f_{\frac{1}{2}} := f(\tfrac{}{2},0,0) + f(-\tfrac{}{2},0,0) + f(0,\tfrac{}{2},0) + f(0,-\tfrac{}{2},0) + f(0,0,\frac{h}{2}) + f(0,0,-\frac{h}{2}),$$

sixth-order convergence can be achieved by first choosing

$$\beta_7 = \frac{109}{15120} \qquad (7.3)$$

and then adding (7.2) to the discretization such that

$$R_{\phi_0} \approx \left\{\frac{-1}{120960}\left(\frac{\partial^6 f}{\partial x^6} + \frac{\partial^6 f}{\partial y^6} + \frac{\partial^6 f}{\partial z^6}\right) + \frac{\kappa}{3024}\left(\frac{\partial^8 u}{\partial x^4 \partial y^4} + \cdots + \frac{\partial^8 u}{\partial y^4 \partial z^4}\right)\right\}h^6$$
$$-\frac{31}{60480}\left(\frac{\partial^6 f}{\partial x^2 \partial z^4} + \cdots + \frac{\partial^6 f}{\partial y^2 \partial z^4}\right)h^6 + C_0^6(x_0, y_0, z_0)h^8. \qquad (7.4)$$

Thus, the sixth-order discrete representation of the equations may be described as

$$\mathbf{H}\Phi = \mathbf{Q}F - F_{Qh}, \qquad (7.5)$$

where the stiffness matrix **H** is composed by (6.2) and the mass matrix is composed by (6.3) with $\beta_7 = \frac{109}{15120}$ and F_{Qh} given in (7.2). Similar sixth-order computational experiments have been demonstrated in [13].

8. Conclusion

We have demonstrated the effectiveness of the finite volume discretization approach in developing efficient higher-order accurate schemes for the three-dimensional Poisson's equation based on the equation error method. Using a more balanced integral form of the equation to formulate the local error expansion provides for an efficient framework for a more complete local flux modeling on the computational domain that ensures local accuracies as well as uniform higher-order accurate convergence of the resulting schemes. In particular, using the 27−point stencil local support for both the mass and stiffness matrices in the discrete equation achieves robust higher-order accurate convergence, and very suitable for large scale eigenvalue problem in 3D due to local accuracy improvements for finer resolutions. Though, both the 19−

point and 27−point local supports yield fourth-order accurate schemes, the 27−point support yields a much better local accuracy as demonstrated through the eigenvalue estimates.

REFERENCES

[1] T. Barth and M. Ohlberger, *Encyclopedia of Computational Mechanics: Finite Volume Methods: Foundation and Analysis*, vol. I, John Wiley & Sons Ltd, Hoboken, USA, 2004.

[2] B. Diskin and J. L. Thomas, *Accuracy analysis for mixed-element finite-volume discretization schemes*, NIA Report NO. 2007-08 (2007).

[3] Q. Du, J. R. Kamm, R. B. Lehoucq, and M. L. Parks, *A new approach for a nonlocal, nonlinear conservation law*, SIAM J. APPL. MATH. **72** (2012), no. 1, 464–487.

[4] S. Gabersek and D. R. Durran, *Gap Flows through Idealized Topography. Part II: Effects of Rotation and Surface Friction*, J. Atmos. Sci. **63** (2006), 2720–2315.

[5] Lixin Ge and Jun Zhang, *Symbolic computation of high order compact difference schemes for three dimensional linear elliptic partial differential equations with variable coeffcients*, J. comput. Appl. Math **143** (2002), 9–27.

[6] K. Ito, Y. Kyei, and Z. Li, *Higher-Order, Cartesian Grid Based Finite Difference Schemes for Elliptic Equations on Irregular Domains* , SIAM J. Sci. Comput. **27** (2005), 346–367.

[7] C. Katz and A. Jameson, *A Comparison of Various Meshless Schemes Within a Unified Algorithm*, 47th AIAA Aerospace Sciences Meeting including The New Horizons Forum and Aerospace Exposition **2009-897** (2009).

[8] R. V. Keer and H. D. Schepper, *Finite Element Approximation for 2nd Order Elliptic Eigenvalue Problems with Nonlocal Boundary or Transition Conditions*, Appl. Math. Comput. **82** (1997), 1–16.

[9] P. Knabner and L. Angermann, *Numerical Methods for Elliptic and Parabolic Partial Differential Equations*, Springer-Verlag, New York, Inc, 2003.

[10] E. P. C. Koh, H. M. Tsai, and F. Liu, *Euler Solution Using Cartesian Grid with a Gridless Least-Squares Boundary Treatment*, AIAA Journal **43** (2005), no. 2.

[11] Y. Kyei, *Space-time finite volume differencing framework for effective higher-order accurate discretizations of parabolic equations*, SIAM J. Sci. Comput. **34** (2012), no. 3, A1432– A1459.

[12] Y. Kyei and K. Edoh, *Higher-order accurate finite volume discretization of helmholtz equations with pollution effects reductions*, Int. J. for Innovation Education and Research **6** (2018), no. 4.

[13] Y. Kyei, J. P. Roop, and G. Tang, *A family of sixth-order compact finite difference schemes for poisson equation*, Adv. Numer. Anal. **Article ID 352174** (2010), 1–17.

[14] S. K. Lele, *Compact finite difference schemes with spectral-like resolution*, J. Comput. Phys. **103** (1992), 1–42.

[15] R. J. LeVeque, *Finite Difference Methods for Ordinary and Partial Differential Equations, Steady State and Time Dependent Problems* , SIAM, 2007.

[16] J. Levesley and D. L. Ragozin, *Local Approximation on Manifolds Using Radial Functions and Polynomials*, International Conference on Curves and Surfaces [4th], Saint-Malo,France, 1-7 July 1999 **Proceedings, Volume 2. Curve and Surface Fitting**, 291–300.

[17] M. Li and T. Tang, *A Compact Fourth-Order Finite Difference Scheme for Unsteady Viscous Incompressible Flows*, J. Sci. Comput. **16** (2001), 29–45.

[18] S. Liang, X. Ma, and A. Zhou, *Finite volume mehtods for eigenvalue problems*, BIT **41** (2001), no. 2, 345–363.

[19] Y. Liu, M. Vinokur, and Z.J. Wang, *Spectral (finite) volume method for conservation laws on unstructured grids V: Extension to three-dimensional systems*, J. Comput. Phys. **212** (2006), 454–472.

[20] F. Lorcher, G. Gassner, and C. D. Munz, *An explicit discontinuous Galerkin scheme with local time-stepping for general unsteady diffusion equations*, J. Comput. Phys. **227** (2008), 5649–5670.

[21] W. H. Mason, *Applied computational aerodynamics*, Text/notes, http://www.dept.aoe.vt.edu/ maxon/Mason f/CAtextTop.html, 1997.

[22] P. Ming and X. Yue, *Numerical methods for multiscale elliptic problems*, J. Comput. Phys. **214** (2006), 421–445.

[23] M. Piller and E. Stalio, *Finite–volume compact schemes on staggered grids*, J. Comput. Phys. **197** (2004), 1064–1094.

[24] J. Santos and P. de Oliveira, *A converging finite volume scheme for hyperbolic conservation laws with source terms*, J. Comput. App. Math. **111** (1999), 239–251.

[25] A. Shiferaw and R. C. Mittal, *An efficient direct method to solve the three dimensional poissons equation*, American J. Comput. Math. **1** (2011), 285 – 293.

[26] W. F. Spotz and G. F. Carey, *A high-order compact formulation for the 3D Poisson equation*, Numer. Meth. Partial Differential Equations **12** (1996), 235–243.

[27] J. C. Strikwerda, *Finite Difference and Partial Differential Equations*, Wadsworth & BrooksCole Advanced Books & Software, 1989.

[28] G. Sutmann and B. Steffen, *High-order compact solvers for the three-dimensional poisson equation*, J. Comput. and Appl. Math. **187** (2006), no. 2, 142 – 170.

[29] A. K. Verma, S. M. Bhallamudi, and V. Eswaran, *Overlapping control volume method for solute transport*, J. Hydr. Engrg. **5** (2000), 308–316.

[30] E. Weinan and B. Engquist, *Multiscale Modeling and Computation*, Notices Of The AMS **50** (2003), no. 9, 1062–1070.

[31] Y. S. Wong and G. Li, *Exact finite difference schemes for solving helmholtz equation at any wavenumber*, Int. J. OF NUMER ANAL AND MODELING, SERIES B **2** (2011), no. 2,
91–108.